9B.5 METHODS FOR IDENTIFYING SYSTEMATIC DIFFERENTIAL REFLECTIVITY (Z_{DR}) BIASES ON THE OPERATIONAL WSR-88D NETWORK

Jeffrey G. Cunningham, W. David Zittel, Robert. R. Lee, and Richard. L. Ice
Radar Operations Center, Norman, OK

Nicole P. Hoban
University of Missouri, Columbia, Missouri

1. INTRODUCTION

1.1 Background

The United States NEXRAD tri-agencies (Departments of Commerce, Transportation, and Defense) recently completed a dual polarization upgrade to the fleet of 160 operational Weather Surveillance Radar - 1988 Doppler's (WSR-88Ds). Differential reflectivity (Z_{DR}), one of several new dual polarization variables, gives hydrometeor shape information and aids in distinguishing hydrometeor type and making quantitative precipitation estimates (QPE). The WSR-88D Radar Product Generator's (RPG) hydrometeor classification algorithm, melting layer detection algorithm (MLDA), and QPE algorithm require unbiased Z_{DR} data to optimize performance.

In August 2010, the Applications Branch of the tri-agency Radar Operations Center (ROC) jointly with the Warning Decision Training Branch conducted an "operational assessment of pre-deployment WSR-88D dual polarization data." The panel of subject matter experts concluded that dual polarization provides significant benefits to forecast and warning operations. Benefits include improved discrimination between precipitation and non-precipitation, discrimination among winter precipitation types, and detection of heavy rain, hail, updrafts, tornadic debris, and the melting layer. Z_{DR} calibration was sufficiently accurate for human interrogation of weather hazards, but there was also a ***potential*** (emphasis added) for better rain estimates through the dual polarization (DP) QPE algorithm, provided that absolute systematic Z_{DR} biases are less than 0.2 dB. Differential reflectivity calibration is important because an absolute systematic Z_{DR} bias of 0.1 to 0.2 dB can produce a QPE error of 10-30% in areas of rain not contaminated by hail or mixed phase precipitation (Illingworth, 2004; Ryzhkov et al., 2005).

Historically, most weather research and operational dual polarization radar users use precipitation targets to calibrate differential reflectivity. Specifically, the preferred method is to vertically point the radar antenna and rotate it through 360° while looking at light precipitation (Bringi and Chandrasekar, 2001). The primary assumption is that raindrops are azimuthally symmetric (i.e., intrinsic Z_{DR} is 0 dB). Regardless of the merits and the quality of the vertically pointing method, WSR-88D antenna design prevents the WSR-88D from pointing vertically.

1.2 Objective

During dual polarization beta testing, independent differential reflectivity calibration monitoring was limited to using light precipitation from volume scans in plan position indicator (PPI) mode. Preliminary results revealed large systematic Z_{DR} biases (> ±0.2 dB) at field test sites (Lee, 2011). This paper provides an overview of the ROC's ongoing efforts to monitor systematic Z_{DR} biases and demonstrates the utility of combined online and offline methods for reducing and/or finding the cause of these biases across the fleet.

2. METHODS FOR ESTIMATING SYSTEMATIC DIFFERENTIAL REFLECTIVITY (Z_{DR}) BIAS

Presently, the WSR-88D system utilizes an internal engineering Z_{DR} calibration process. This is a dynamic calibration method in which a bias correction (Δ_{cal}) is applied to measured differential reflectivity values (ZDR_{meas}), such that:

$$ZDR_{Level2} = ZDR_{meas} - \Delta_{cal}, \quad (1)$$

where ZDR_{Level2} refers to radar data that has been formatted for transmission from the Radar Data Acquisition hardware to the RPG (Interface Control Document for the RDA/RPG) and ZDR_{meas} is the calculated Z_{DR} value from the H (horizontal) and V (vertical) powers received. Ideally, the engineering calibration process estimates the "*total*" systematic Z_{DR} bias accurately (i.e., $\Delta_{cal} = \Delta_{total}$). This calibration process has no single "knob" for a technician to adjust system performance. Accurately measuring the split power between the H and V channels, the transmit path and receive path losses for each channel, and the antenna gain for H and V are important for the engineering calibration process to work correctly.

* *Corresponding Author*: Dr. Jeffrey G. Cunningham, Radar Operations Center, 1200 Westheimer Drive Norman, OK 73069
e-mail: jeffrey.g.cunningham@noaa.gov

The views expressed are those of the authors and do not necessarily represent those of the United States Air Force.

Radar measured Z_{DR} values from nearby external targets with intrinsic $Z_{DR} = 0$, such as light precipitation (Δ_{precip} , as described in Section 2.2) and Bragg scatter (Δ_{Bragg}, as described in Section 2.3), enable observational monitoring of the total system Z_{DR} bias, Δ_{total}. The ROC is routinely monitoring systematic Z_{DR} biases across the fleet with these "online" and "offline" observational methods. In parallel with ROC observational monitoring, the National Severe Storms Laboratory (NSSL), and the National Center for Atmospheric Research (NCAR) are jointly investigating Z_{DR} calibration related issues. Specifically, NCAR is investigating the use of cross-polar power calibration method on the WSR-88D (Hubbert et al. 2003; Ice et al., 2013) and NSSL is conducting component level investigations and participating in routine fleet-wide data quality reviews.

2.1 Contributions to System Differential Reflectivity Bias

Following Zrnić et al. (2006), Holleman et al. (2010) and A. Heck (2013, personal communication) the total systematic Z_{DR} bias is

$$\Delta_{total} = \Delta Rx + \Delta Tx, \quad (2)$$

where ΔRx is the receive path bias and ΔTx is the transmit path bias. Receive path bias is

$$\Delta Rx = rx_{bias} + ant_{bias}, \quad (3)$$

where rx_{bias} is the receiver contribution and ant_{bias} is a one-way antenna contribution. The transmit path bias is

$$\Delta Tx = tx_{bias} + ant_{bias}, \quad (4)$$

where tx_{bias} is the transmitter contribution and ant_{bias} is a one-way antenna contribution. The total systematic Z_{DR} bias can be rewritten as

$$\Delta_{total} = rx_{bias} + tx_{bias} + 2 * ant_{bias}. \quad (5)$$

Transmitter, receiver, and antenna (two-way) components influence total system bias. ZDR_{meas} values from the sun (described in Section 2.4) only indicate the receive path bias, ΔRx. With an estimate of the total system bias and a receive path estimate, one can derive the transmit path bias:

$$\Delta Tx = \Delta_{total} - \Delta Rx. \quad (6)$$

Section 2.2 and 2.3 describe how the ROC uses online and offline methods to monitor the total system Z_{DR} bias from light precipitation and Bragg scatter targets, Δ_{precip} and Δ_{Bragg}, respectively. Section 2.4 describes how the ROC monitors the receive path bias (ΔRx) using sunspikes.

2.2 Total System Z_{DR} Bias Estimates with Light Precipitation (Scanning Method)

A. Ryzhkov developed a method that uses operational scanning strategies to estimate Δ_{total} with light rain (2011, personal communication). The technique uses reflectivity data at elevation angles greater than 1° and beginning 20 km from the radar to avoid ground clutter. Two filters are applied to the reflectivity data: signal-to-noise ratio (SNR) > 20 dB and correlation coefficient (ρ_{hv}) > 0.98 to make sure strong signal is processed in the uniform rain region. To make sure that data processed is rain, radar bins are restricted to be at least 1 km below the bottom of the melting layer, as determined with the MLDA (B. Klein, 2013, personal communication). Next, the reflectivity data is sorted between 19 and 30.5 dBZ into six reflectivity categories of 2 dB width that are centered at Z = 20, 22,…30 dBZ. The median value of all the Z_{DR} values in each category is computed as long as there are at least 200 data points per category. The Z_{DR} values for each reflectivity category, listed in Table 1, are subtracted from the corresponding median Z_{DR} value in each reflectivity category. These empirical data were derived from disdrometer data collected in Oklahoma (Schuur et al., 2001; Schuur et al., 2005). The total systematic Z_{DR} bias, Δ_{precip}, is computed by averaging the six empirically corrected categories together. Δ_{precip} for each volume scan is averaged over a 12 volume scan running window to ensure statistical stability.

It is possible that the weak reflectivity regions are near or on the fringe of strong convective areas which may contaminate the light reflectivity region with large drops. These large contaminating drops do not meet the small drop and Z_{DR} value assumptions about light rain. Therefore, it was necessary to develop a convective versus stratiform precipitation discriminator so that the influence of convective events could be reduced.

Two volume tests are applied to decrease the chance of big drop contamination. The first test relies on the assumption that convection lofts many large drops above the melting level (J. Krause, 2013, personnel communication). At far range, above the melting level, if fewer than 40 radar bins have reflectivity values of 40 dBZ or more, the sample is classified as stratiform. The 40 bin threshold is determined from a one month empirical study which used data from all WSR-88D sites that had rain and valid Z_{DR} measurements.

The second test using data from the same study focuses on data near the radar below the melting level. All radar bins are counted which had SNR > 20 dB, ρ_{hv}

> 0.98, and reflectivity values between 10 and 30 dBZ. The same criteria are applied to reflectivity values greater than 30 dBZ. If 80% or more of the reflectivity values were from the 10 and 30 dBZ reflectivity category, then the sample is classified as stratiform. If both tests classify a volume as stratiform the volume is designated as stratiform and retained for Δ_{precip} calculations.

A simple melting level algorithm supports these two tests. Correlation coefficient values between 0.88 and 0.98 are found between ranges 37 km (20 nmi) and 167 km (90 nmi) from the radar. Bins are restricted to having reflectivity values of 25 dBZ or more. A 15-bin moving average is taken along each radial. If 12 or more of the 15 bins met the filter criteria, the range was recorded. The melting level for that radial is set to the average range of the saved ranges. The melting level for the sample is computed as the average range of all the radials that met the filter criteria.

Automated data processing 1) collects Z_{DR} values from each radar volume scan during rain events from all radar sites, 2) divides the data samples up into three hour blocks; 3) computes the Δ_{precip}, correcting light rain Z_{DR} values by the empirically derived values; 4) classifies each sample as stratiform or convective using Level II radar data; and 5) processes the stratiform cases into WSR-88D network national maps and histograms.

With the light precipitation scanning method described here the authors assume that intrinsic Z_{DR} values of light rain can be accurately corrected to zero dB for a large number of radar volumes (i.e., over a long duration) and that the convective/stratiform classification tests accurately separate the two precipitation modes. These are challenging assumptions to maintain; therefore, the authors also explored observing Bragg scatter to estimate Δ_{total}. Bragg scatter is not susceptible to large drop contamination and drop-size distribution variability is not a factor.

2.3 Total System Z_{DR} Bias Estimates with Bragg Scatter (Scanning Method)

The authors investigated the feasibility of detecting Bragg scatter on the operational fleet of WSR-88Ds in order to determine systematic Z_{DR} biases. Bragg scattering is typically found at the top of the convective boundary layer (CBL) where mixing of moist and dry air occurs (Melnikov et al., 2011). The temperature and moisture variations cause density and refractive index perturbations, enhancing clear air return of the radar beam. Melnikov et al. often found Bragg scatter during maximum surface heating when thermal plumes occur most frequently.

Figure 1 shows a layer of Bragg scattering at the top of the CBL and on top of a layer of biota and ground clutter. It demonstrates the near zero nature of the Z_{DR} values associated with Bragg scattering compared to the high Z_{DR} values of biota and ground clutter. The turbulent eddies (diameter ≈ 5 cm) that cause Bragg scattering should have no preferred orientation (i.e., distributed randomly in the plane of polarization); therefore, Bragg scattering should have an intrinsic Z_{DR} of zero (Melnikov et al, 2011).

Unlike the test-bed WSR-88D (KOUN) used in Melnikov's study, operational WSR-88Ds do not scan above 19.5° elevation in any volume coverage pattern (VCP) and not above 4.5° elevation when operating in clear air mode (VCPs 31 or 32 described in Appendix). Each VCP is constrained to a limited number of pulses (short dwell times) per radial, predefined elevation increments of 1° (clear-air mode), and range sampling at 0.25 km. Besides scanning above 20° in elevation, using 0.25° elevation increments, increasing dwell times, and doubling the sampling rate, Melnikov et al., used special signal processing techniques for estimating Z_{DR}.

For proof of concept the authors found Bragg scattering on the Norman, OK operational WSR-88D (KTLX) on days Melnikov had found on the KOUN radar (2013, personal communication). They expanded the search to include other WSR-88Ds operating in VCP 32 or VCP 21. Examples of Bragg scattering were observed at diverse sites such as Portland, Ore., Caribou, ME, Morehead City, NC and Lubbock, TX (not shown).

An example of Bragg scattering seen on the operational Little Rock, AR WSR-88D (KLZK) is shown in Figure 2. By definition Bragg scattering has weak returns (<10 dBZ), Z_{DR} in the absence of large systematic bias is near zero, ρ_{hv} is high (>0.98), and differential phase (Φ_{dp}) should be near the value of the initial system differential phase (ISDP) of 25°. Contamination from biota and clutter, and returns below the minimum detectable signal at distances far from the radar make Bragg scattering more easily detectable at elevation angles of 2.5° and higher. As in Melnikov's study, midday was most favorable for finding Bragg scattering.

To identify Bragg scatter automatically, the ROC applied filters to base data moments (reflectivity, SNR, velocity, and spectrum width) and to dual polarization parameters (ρ_{hv} and Φ_{dp}) to ensure that only weak signals were included and to reduce contamination due to ground targets or biota (Hoban et al., 2013). Histograms were generated from the Z_{DR} values resulting from the intersection of all the filters for a one-hour period. Each histogram had to have at least 35,000 points and satisfy the Yule-Kendall index symmetry test with a value of ≤ 0.1 (Wilks, 2006; Hoban et al., submitted 2014). Histograms (by radar site) of the Bragg scattering are examined to determine

the modal Z_{DR} value which, ideally, should be zero. For example, the difference between zero and the histogram peak is approximately equal to 0.75 dB ($\Delta_{Bragg} \cong 0.75\ dB$), which is the systematic Z_{DR} bias for KLZK on 12 May 2013 (Fig. 3).

2.4 Receive Path Bias Estimates with Sunspikes (Scanning Method)

Since its deployment, the WSR-88D fleet has regularly observed electromagnetic radiation from the sun (i.e., "sunspikes"). These observations are especially noticeable in national mosaics of composite reflectivity around sunrise and sunset (not shown). Sunspikes are observed in all base moments and in the dual polarization variables. Figure 4 shows an example of a sunspike from the Upton, NY, WSR-88D (KOKX) for Z, Z_{DR}, ρ_{HV}, and Φ_{DP}.

High resolution imaging of the sun at λ = 11 cm indicates no detectable linear polarization but may have limited circular polarization due to sunspots (Lang, 1977). If the sun is unpolarized, it follows that the intrinsic differential reflectivity of a sunspike ($ZDR_{intrinsic}$) should be 0 dB unless there is a receiver or antenna bias. For sunspikes the following equation applies:

$$ZDR_{meas} = ZDR_{intrinsic} + rx_{bias} + ant_{bias}, \quad (7)$$

which is simply

$$ZDR_{meas} = rx_{bias} + ant_{bias}. \quad (8)$$

In practice, the RDA applies a dynamic systematic correction (Δ_{cal}) to the measured differential reflectivity values (ZDR_{meas}). Because the transmit path plays no role in the sun's Z_{DR} values, these values may be artificially biased away from zero. Therefore it becomes necessary to remove the Δ_{cal} from the sunspike Z_{DR} values:

$$ZDR_{Level2} = ZDR_{meas} - \Delta_{cal},$$

becomes

$$ZDR_{meas} = ZDR_{Level2} + \Delta_{cal} =$$

$$rx_{bias} + ant_{bias} = \Delta Rx.$$

When combined with a full bias measurement, such as Δ_{precip} or Δ_{Bragg}, useful information about the source of Z_{DR} errors may be obtained. Holleman et al., (2010) used this approach for monitoring Z_{DR} biases on two European 5 cm radars.

The Upton, NY radar provided an excellent opportunity to conduct a proof-of-concept test. After KOKX was converted to dual polarization, $\Delta_{precip} \cong 0.6\ dB$. After a bull gear failure in mid-November 2012, ROC electronic technicians dismantled and reassembled the dual polarization components and completed a hardware calibration. Afterwards, $\Delta_{precip} \cong -0.2\ dB$, a swing of about 0.8 dB. Sunspike ZDR_{Level2} before the bull gear failure showed a bias between 0.9 and 1.0 dB. After the bull gear replacement the sunspike ZDR_{Level2} bias was about 0.1 dB, again a shift of about 0.8 dB. Figure 5a shows sunspike ZDR_{Level2} values out to 100 km from KOKX on November 10, 2012. The average values are near 0.9 dB. Figure 5b shows sunspike ZDR_{Level2} values on December 13, 2012. The average value here is close to 0.0 dB. Because the proof-of-concept test showed promising results, tools were developed to automatically look for sunspikes and compute sunspike ZDR_{meas} (with Δ_{cal} removed).

The sunspike method for monitoring receive path biases does have limitations. The method, as currently implemented, relies on windows of opportunity which requires the radar to be operating in VCP 32 and the sun to be at a low angle. Rarely do the azimuthal and elevation positions of both the sun and the radar align perfectly. The precision with which the radar's position is known is 0.044° either azimuthally or vertically. Temperature anomalies, most often inversions, may cause the sun to appear at an angle different from astronomical calculations. Also, high latitude radar sites may not see the sun in winter months.

3. FLEET STATISTICS

Results from two observational monitoring processes (Δ_{precip} and Δ_{Bragg}) suggest that the combination of the existing dynamic hardware Z_{DR} calibration process (Δ_{cal}) and current maintenance procedures are not yet able to prevent large systematic Z_{DR} biases in many cases. Figure 6 shows monthly fleet-wide histograms of median Δ_{precip} for 3-hour stratiform events. The maximum contribution from any single radar site is 3% (Table 2). Ideally, in any event a radar should have $|\Delta_{precip}| \leq 0.2\ dB$. Between April and July 2013, 56-59% of 3-hour stratiform events identified across the fleet had a $|\Delta_{precip}| \leq 0.2\ dB$. Conversely, 41-44% of stratiform events identified across the fleet have a $|\Delta_{precip}| > 0.2\ dB$.

Figures 7-10 show national maps of Δ_{precip} computed for each site for April – July 2013. Figure 11 shows the WSR-88D site identifier for reference. Data are made up of three hour blocks and represent only the stratiform events. Systematic biases are color coded with $|\Delta_{precip}| \leq 0.1\ dB$ as green, $0.1\ dB <$

$|\Delta_{precip}| \leq 0.2\ dB$ as yellow, and $|\Delta_{precip}| > 0.2\ dB$ as red. Sites with $\Delta_{precip} < -0.2\ dB$ have a black box around the number. Sites labeled "NaN" and colored gray did not have enough data / rain to compute a Δ_{precip} value.

Monthly Δ_{precip} values vary from site to site and month to month, but most sites have a consistently high or low bias. Between April and July 2013, 23-29% of sites had $|\Delta_{precip}| \leq 0.1\ dB$, 24-32% of sites were $0.1\ dB < |\Delta_{precip}| \leq 0.2\ dB$, 42-46% of sites had $|\Delta_{precip}| > 0.2\ dB$. Sites with $\Delta_{precip} < -0.2\ dB$ are especially of interest (17-27%), since large drop contamination is unlikely to have contributed to the negative Δ_{precip} values.

4. WSR-88D SITE CASE STUDIES

Detailed site-by-site reviews are beginning to help meteorologists, engineers, and technicians understand hardware, maintenance, and procedural issues that influence systematic Z_{DR} biases. The ROC actively works with field sites to improve systematic Z_{DR} biases. Here, we review time series of relevant Z_{DR} calibration data for KBOX, KRAX, KLZK, and KCBW (Figs. 12-15). Available data for Δ_{precip}, Δ_{Bragg}, system and derived ΔRx and ΔTx, and subcomponents ($rx_{bias}, tx_{bias}, and\ ant_{bias}$) are plotted as scatter points. Total bias estimates ($e.g.\ \Delta_{precip}, \Delta_{Bragg}$) should be near zero for unbiased systems. ΔRx, ΔTx and subcomponents ($rx_{bias}, tx_{bias}, and\ ant_{bias}$) may be non-zero, so long as the combination of terms (Eq. 2 or 5) yields a zero sum. Here are few examples of the different types of challenges the ROC is aware of across the fleet.

4.1 Boston, MA (KBOX)

The following case demonstrates how WSR-88D adaptation data changes can influence systematic Z_{DR} biases. Between January and late February 2013, KBOX had an acceptable systematic bias ($\Delta_{precip} < 0.1\ dB$ in Fig. 12). However, in late February 2013, KBOX began exhibiting a $\Delta_{precip} \cong 0.4\ dB$. Upon investigation, the ROC discovered that the ant_{bias} changed as a result of a manual change to the RDA adaptation parameter A031 (i.e., ant_{bias}). Antenna bias values (ant_{bias}- blue sideways triangles) were not available for plotting until after late February (Fig. 12). Derived ΔRx from sunspikes (red stars) and system ΔRx (red circles) should be approximately equal to each other. Derived and system ΔRx are not equal to one another for KBOX between February and April 2013 (Fig. 12). Similarly, the derived and system ΔTx were not equal to one another during the same period. The difference between the derived and system biases for both the transmit and receive path was each approximately equal to the ant_{bias}. Therefore, the incorrect ant_{bias}setting contributed twice to the Δ_{cal} (Eq. 5), thus causing the system to bias ZDR_{Level2} values high.

A site electronics technician ran a routine sun scan, but the sun scan generated an incorrect ant_{bias}value. In late April, ROC Hotline technicians suggested the technician change the A031 value back to the original setting prior to late February. Upon changing A031, KBOX began operating with acceptable Δ_{precip}. Changing the A031 parameter back to the original setting is only a temporary measure, as the routine sun scan procedure should not have generated an incorrect ant_{bias} measurement. The ROC and NSSL continue to investigate the source of the ant_{bias} error.

4.2 Raleigh, NC (KRAX)

For May through June 2013, Raleigh experienced a stable, but unacceptable $\Delta_{precip} \leq -0.50\ dB$ (Figs. 7-10 and Fig. 13). The alternative Bragg scatter method indicated a $\Delta_{Bragg} \cong -0.5\ dB$ for May and June (Fig. 13), which is consistent with the light precipitation method. In late June, ROC and site electronic technicians worked together to replace several major dual polarization hardware components, including but not limited to the RF pallet and 30 dB attenuator. After repair completion, ROC technicians immediately conducted a full hardware calibration on the KRAX WSR-88D system. Beginning in late June, KRAX showed improvement, exhibiting $-0.4 < \Delta_{precip} < -0.2\ dB$. Prior to late June, the derived and system ΔRx were slightly different, indicating that system receiver bias or antenna bias were possibly not set correctly. Derived ΔTx were unavailable to compare with system ΔTx. Although KRAX's systematic Z_{DR} bias has improved, Δ_{precip} continues to be less than -0.2 dB (outside preferred limits for DP QPE).

4.3 Little Rock, AR (KLZK)

The Little Rock, AR WSR-88D (KLZK) system exhibited unstable systematic Z_{DR} biases, as indicated by $\Delta_{precip} \cong 0.36\ dB$ in April, 0.69 dB in May, 0.57 dB in June, and 1.58 dB in July (Figs. 7-10 and Fig 14). In late May, the alternative Bragg scatter method indicated a $\Delta_{Bragg} \cong 0.75\ dB$ during a time when the light precipitation method was unable to provide a bias estimate due to lack of light precipitation. KLZK derived and system ΔRx estimates are approximately equal to and consistent with one another; however, during the same period the derived and system ΔTx are

not equal to one another (the derived ΔTx remains relatively constant compared to the increasingly negative system ΔTx), implying that KLZK hardware sensors are not determining the appropriate system tx_{bias} correction. The ROC is continuing to investigate the problems associated with this WSR-88D.

4.4 Caribou, ME (KCBW)

The Caribou, ME (KCBW) WSR-88D site has maintained a stable and near zero Δ_{precip} and Δ_{Bragg} for at least four months (Figs. 7-10 and Fig. 15). Almost all Z_{DR} calibration parameters remained near zero between April and early August. Available maintenance logs indicate that few major adjustments have been made to KCBW since the radar was upgraded to dual polarization.

4.5 Summary

Other site reviews (not shown) demonstrate additional challenges of calibrating Z_{DR}. Using maintenance and system status logs, the ROC has correlated sudden Z_{DR} bias changes to certain maintenance actions. The cases presented here represent a small sample of site-specific data collected since the fleet upgrade to dual polarization.

5. CONCLUSION

Three observational systematic differential reflectivity bias monitoring methods were described in detail. The first method relies on external light precipitation targets in volumetric data to estimate the total systematic Z_{DR} bias. An alternative volumetric data method uses Bragg scatter targets instead of light precipitation. Large drops do not contaminate Bragg scatter; however, filtering out biota is especially important. Finally, the authors demonstrated the use of sunspikes to estimate receive path Z_{DR} bias.

The authors compared the performance of the WSR-88D's internal systematic Z_{DR} calibration process (Δ_{cal}) with the light precipitation method (Δ_{precip}) and the Bragg scatter method (Δ_{Bragg}). Geographical and meteorological conditions restrict the fleet-wide usage of the three techniques in various ways (e.g., low sun angle at high latitude, infrequent light rain, or low boundary layer moisture, etc.). According to the light precipitation method, from April to July 2013 54-58% of the sites operated with a systematic Z_{DR} bias less than or equal to 0.2 dB and 42-46 % of the sites operated with a systematic Z_{DR} bias greater than 0.2 dB. For the cases presented, the Bragg scatter method generates total system Z_{DR} bias estimates similar in value to the light precipitation method ($\Delta_{Bragg} \cong \Delta_{precip}$). The authors intend to further refine the Bragg scatter method and apply it to the entire fleet.

The observation that more than half of the sites are experiencing biases of less than 0.2 dB at this early stage is encouraging given the technical challenges associated with establishing and maintaining accurate calibration baselines for differential reflectivity. The NEXRAD program experienced analogous issues with reflectivity calibration after the initial deployment of the WSR-88D. Achieving the required 1 dB accuracy in reflectivity was not always achieved in practice and was not well established until the ROC began actively monitoring network performance using site comparison tools and online parameter monitoring (Ice et al., 2005). It is quite likely such an active monitoring effort using the tools described here will be necessary to establish and maintain the desired accuracy (0.1 dB) in differential reflectivity for QPE. Meanwhile, trained forecasters can use relative maximums and minimums in the Z_{DR} field to detect tornadic debris signatures, the presence of large hail, winter precipitation transition zones, and early recognition of strong updrafts.

ACKNOWLEDGMENTS

The authors thank Dr. Valery Melnikov (NSSL), Jami Boettcher (Warning Decision Training Branch) and colleagues within the ROC for reviewing this paper. Special thanks to Dr. Melnikov for suggesting the Bragg scatter technique and to Adam Heck and Dr. Dusan Zrnić for discussions on calibration equations.

REFERENCES

Bringi, V. N. and V. Chandrasekar, 2001: *Polarimetric Doppler Weather Radar: Principles and Applications*. Cambridge University Press, 636 pp.

Hoban, N. P., J. G. Cunningham, W. D. Zittel, 2013: Using Bragg Scatter to Estimate Systematic Differential Reflectivity Biases on Operational WSR-88Ds. *Real-world Research Experience for Undergraduates at the National Weather Center*.

Hoban, N. P., J. G. Cunningham, W. D. Zittel, submitted 2014: Using Bragg Scatter to Estimate Systematic Differential Reflectivity Biases on Operational WSR-88Ds. *30th Conference on Environmental Information Processing Technologies,* Atlanta, GA. Amer. Meteor. Soc.

Holleman, Iwan, A. Huuskonen, R. Gill, P. Tabary, 2010: Operational monitoring of radar differential reflectivity using the sun. *J. Atmos. Oceanic Technol.,* **27**, 881-887.

Hubbert, J. C., V. N. Bringi, and D. Brunkow, 2003: Studies of the Polarimetric Covariance Matrix. Part I: Calibration Methodology, *J. Atmos. Oceanic Technol.*, **20**, 696-706.

Ice, R. L., D. A. Warde and F. Pratte, 2005: Investigating External and Dual Polarization Calibration Options for the WSR-88D, *32nd Conference on Radar Meteorological,* Albuquerque, NM. Amer. Meteor. Soc.

Ice, R. L., A. K. Heck and J. G. Cunningham, 2013, Polarimetric Weather Radar Calibration – Engineering Challenges, *36th Conference on Radar Meteorology,* Albuquerque, NM. Amer. Meteor. Soc.

Illingworth, A., 2004: Improved Precipitation Rates and Data Quality by Using Polarimetric Measurements. *Weather Radar: Principles and Advanced Applications*. Springer, 130-166.

Lang, Kenneth R., 1977: High resolution polarimetry of the sun at 3.7 and 11.1 cm wavelengths. *Solar Physics,* **52**, 63-68.

Lee, Robert R., 2011: DQDP Subcommittee Decision on Deployment of the Dual Polarization Upgrade. Data Quality Committee Minutes.

Melnikov, V., R. J. Doviak, D. S. Zrnić, and D. J. Stensrud, 2011: Mapping Bragg scattering with a polarimetric WSR-88D. *J. Atmos. Oceanic Technol.*, **28,** 1273-1285.

Radar Operations Center, Applications Branch, 2010: Operational Assessment of Pre-deployment WSR-88D Dual polarization Data, 58 pp. (Available on-line at http://www.roc.noaa.gov/wsr88d/publicdocs /AppsDocs/OpsAssessment28Dec2010.pdf.)

Ryzhkov, A. V. et al, 2005, Calibration Issues of Dual-Polarization Radar Measurements, *J. Atmos. Oceanic Technol.*, **22**, 1138 - 1155.

Schuur, T. J., A. V. Ryzhkov, and D. S. Zrnić, 2001: A statistical analysis of 2D-video-disdrometer data: impact on polarimetric rainfall estimation. Preprints, *30th International Conference on Radar Meteorology,* Munich, Germany. Amer. Meteor. Soc.

Schuur, T. J., A. V. Ryzhkov, and D. R. Clabo, 2005: Climatological analysis of DSDs in Oklahoma as revealed by 2D-video disdrometer and polarimetric WSR-88D radar. Preprints, *32nd Conference on Radar Meteorology,* Albuquerque, NM. Amer. Meteor. Soc.

Wilks, D. S., 2006: *Statistical Methods in the Atmospheric Sciences*. 2nd ed. Elsevier Inc.

WSR-88D Radar Operations Center, 2012: Interface Control Document for the RDA/RPG, 115 pp.

Zrnić, D. S., V. M. Melnikov, and J. K. Carter, 2006: Calibrating Differential Reflectivity on the WSR-88D. *J. Atmos. Oceanic Technol.,* **23**, 944-951.

APPENDIX. DESCRIPTION OF VOLUME COVERAGE PATTERNS VCP 31 AND VCP 32

Initially, to develop the proofs of concept for finding Bragg scattering and sunspikes, sites with Z_{DR} biases away from zero were examined during periods of quiescent weather using the clear air volume coverage patterns (VCPs) 31 and 32. Both VCP 31 and 32 consist of sequential plan position indicator (PPI) scans from 0.5° to 4.5° elevation in one degree steps. For VCP 31 the lowest three elevation consist of pairs of scans (split cuts) at each elevation. The first (i.e. surveillance) scan has a low pulse repetition frequency (PRF) of about 322 Hz (63 pulses). The second (i.e., Doppler) scan has a slightly higher PRF (~446 Hz and 87 pulses). For these three elevations the dual polarization parameters are derived from the surveillance scan, and sunspikes are not range folded. The elevations at 3.5° and 4.5° consist of a single Doppler scan using a PRF of ~446 Hz with 87 pulses. The dual polarization parameters are derived from these Doppler scans, but the sunspikes appear as range folded. In VCP 32 the lower two elevations are split cuts consisting of a low PRF surveillance scan (~322 Hz and 64 pulses) followed by a high PRF (~1014-1282 Hz and > 200pulses) Doppler scan. For these two elevations the dual polarization parameters are derived from the surveillance scan. For elevation angles above 1.5°, each radial consists of 11 pulses at a low PRF followed by >200 pulses at a high PRF. The dual polarization fields are derived from the high PRF data at these elevations. As with VCP 31, VCP 32 sunspike data from Doppler scans are range folded and, thus, unusable for the study. To minimize ground clutter contamination and nonstandard refraction, the 1.5° elevation angle (2.5° for VCP 31) was chosen over the lowest elevation to look for sunspikes. A feature of the split cuts is that the azimuthal resolution is 0.5° rather than 1°, useful for reducing errors when matching radar and sun positions.

TABLES

Table 1 - Average empirical values of Z_{DR} corresponding to Z bins at S band as established by Ryzhkov (2011, personal communication).

Z (dBZ)	20	22	24	26	28	30
ZDR (dB)	0.23	0.27	0.32	0.38	0.46	0.55

Table 2. Scanning Precipitation Method Fleet-wide Histogram Data

Month	# of Unique Sites	Total # of Events	Max Event Contribution by a Single Site
April	82	296	10 (3%)
May	100	503	16 (3%)
June	116	568	15 (3%)
July	129	751	15 (2%)

Table 3. Scanning Precipitation Method Map Metadata

Systematic Z_{DR} bias	Color Code	April	May	June	July
$\lvert \Delta_{precip} \rvert \leq 0.1\ dB$	Green	24 (29%)	23 (23%)	36 (31%)	34 (26%)
$0.1\ dB < \lvert \Delta_{precip} \rvert \leq 0.2\ dB$	Yellow	22 (27%)	31 (31%)	28 (24%)	41 (32%)
$\Delta_{precip} > 0.2\ dB$	Red	19 (23%)	19 (19%)	32 (28%)	32 (25%)
$\Delta_{precip} < -0.2\ dB$	Red & Boxed	17 (21%)	27 (27%)	20 (17%)	22 (17%)
Total Sites		82	100	116	129

FIGURES

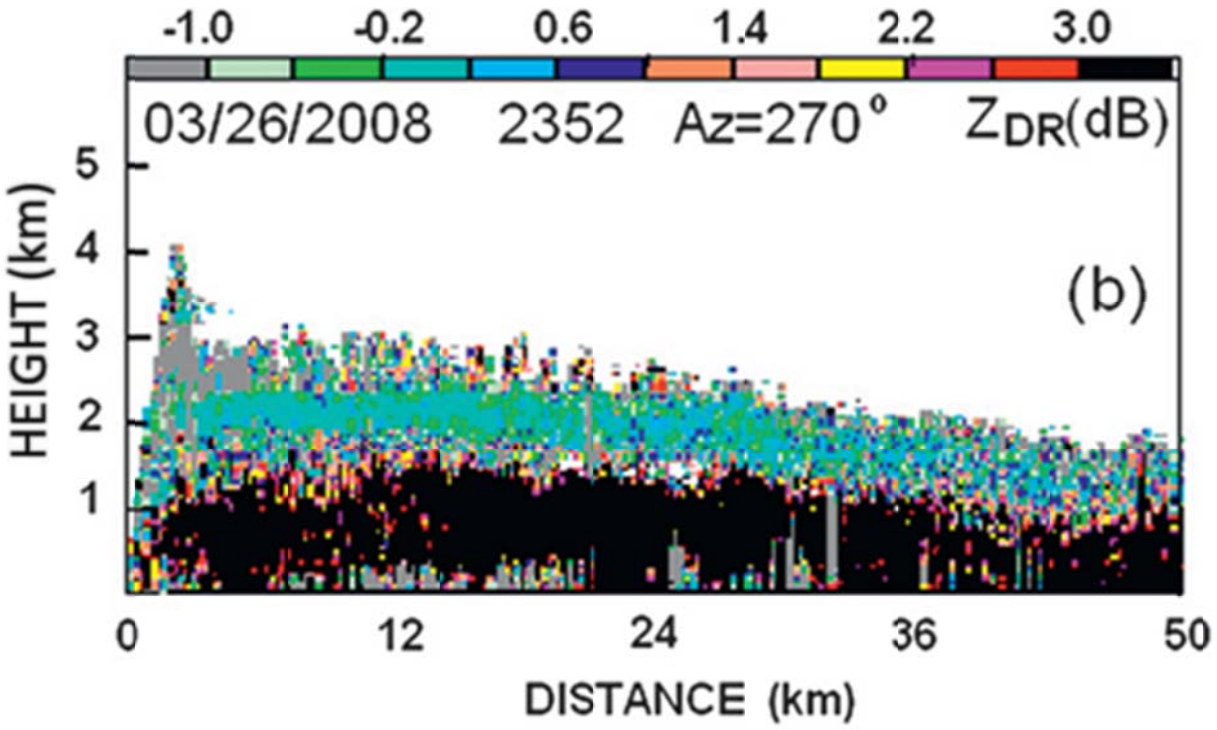

Figure 1. Vertical cross section of Z_{DR} (dB) above Norman, OK at 0000 UTC 21 Feb. 2008 (Melnikov et al., 2011).

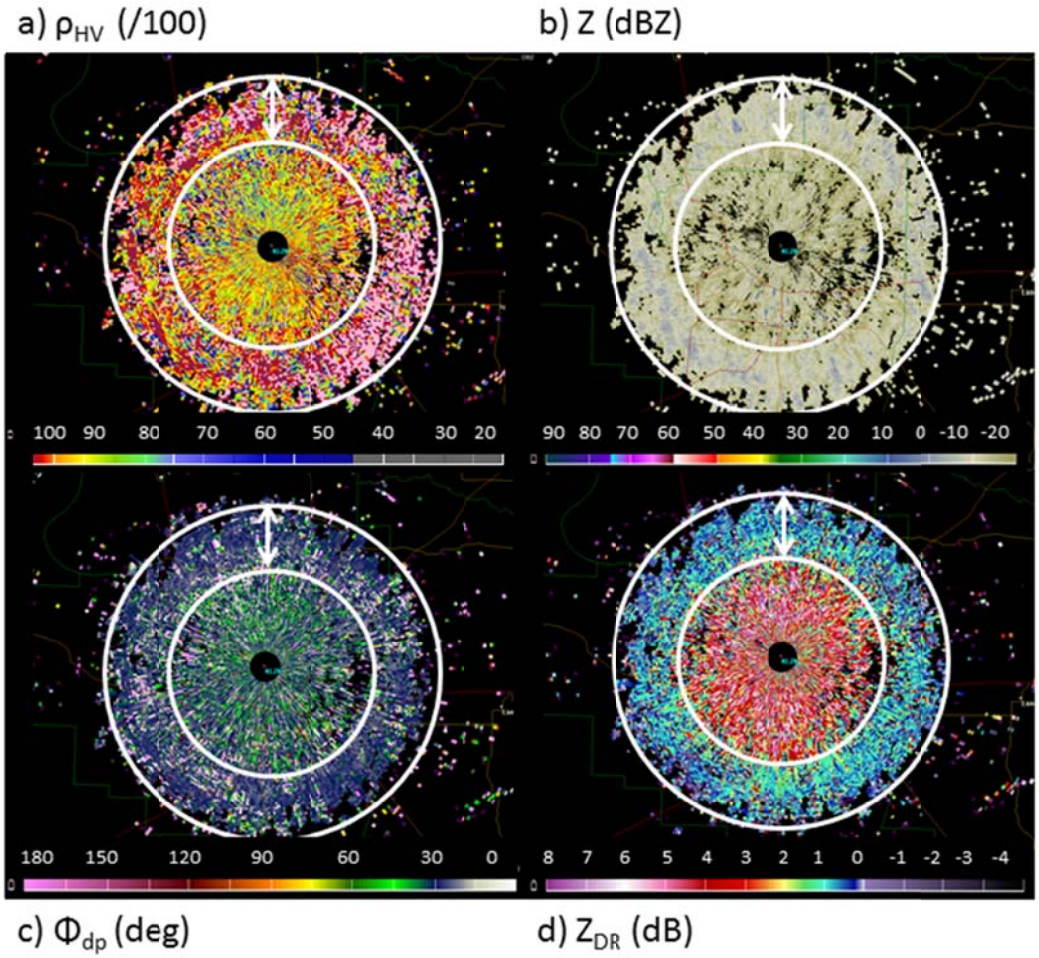

Figure 2. Image from the operational Little Rock, AR WSR-88D (KLZK) on 12 May 2013, at 15:43:08 UTC at 3.5° elevation. Panel a) is correlation coefficient (**/100**), b) is reflectivity (dBZ), c) is differential phase (deg) and d) is differential reflectivity (dB). The annulus in each panel shows the region with Bragg scattering (Hoban et al., 2013). The annulus rings are 15 and 25 km.

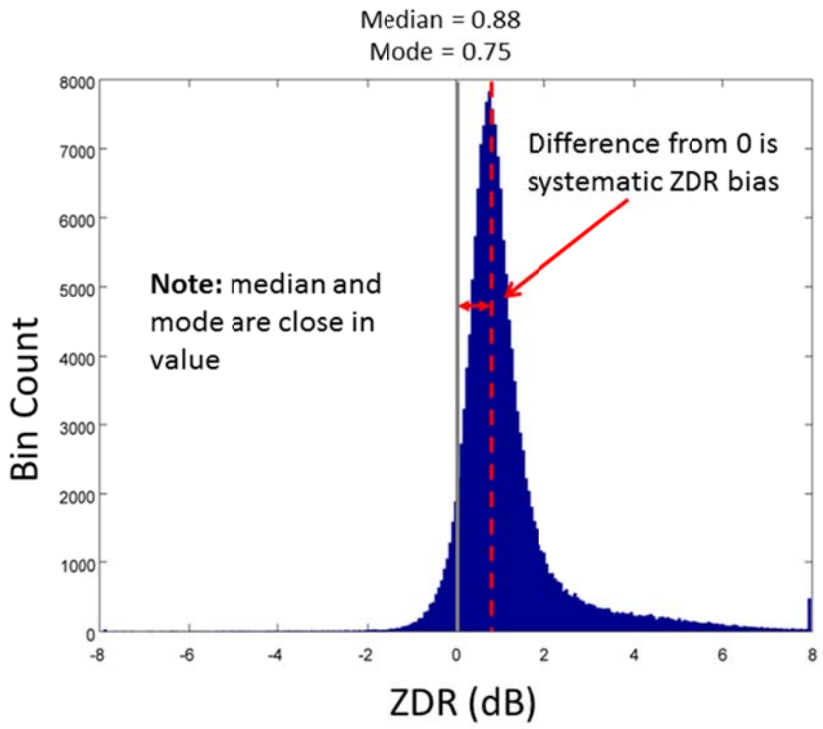

Figure 3. Histogram of differential reflectivity (Z_{DR}) from Bragg scatter filtered bins at Little Rock, AR WSR-88D (KLZK) on 12 May 2013. The mode of the distribution represents the systematic Z_{DR} bias (Hoban et al., 2013).

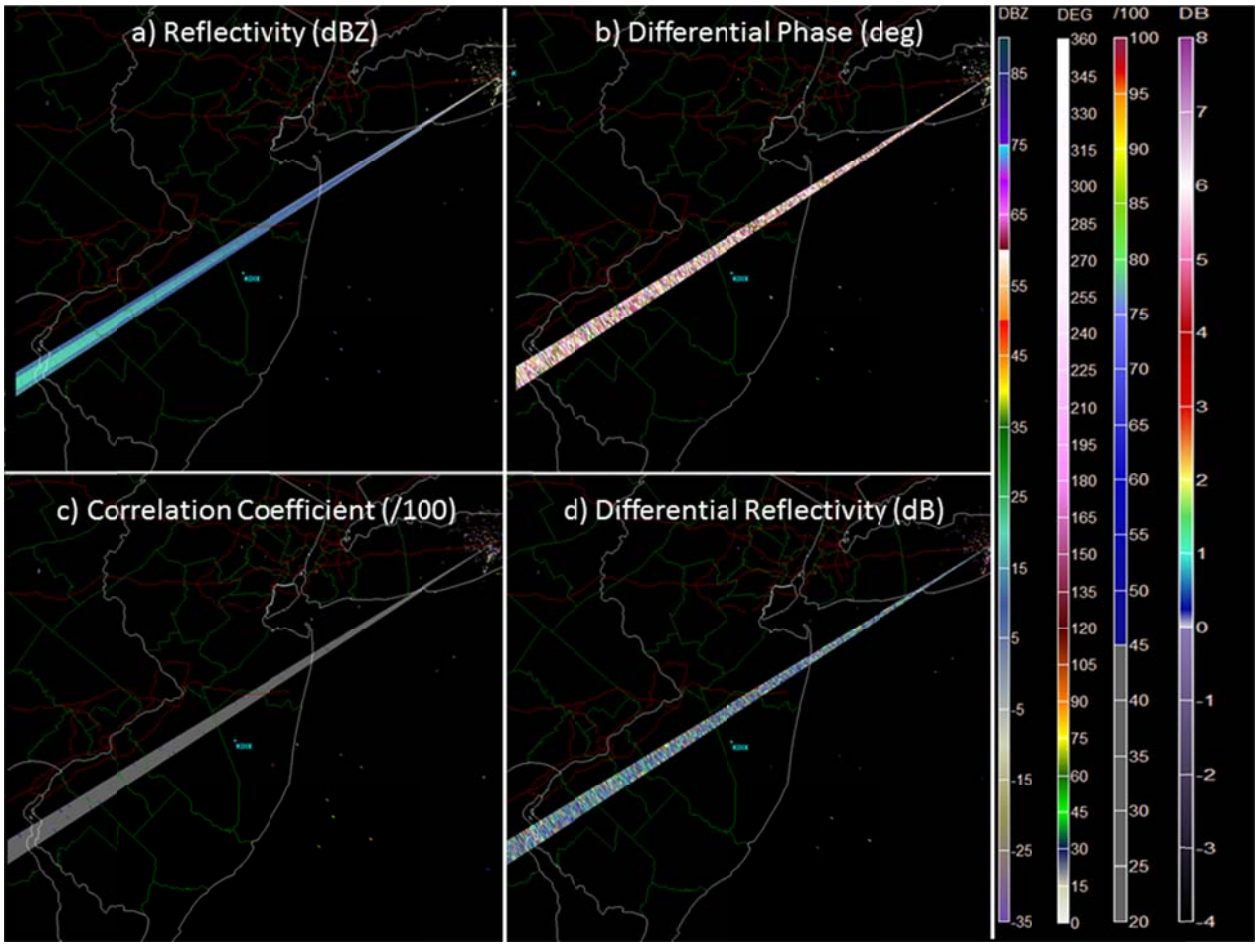

Figure 4. Example of a sunspike observed around sunset at the Upton, NY WSR-88D on December 13, 2012 at 21:11 UTC. Upper left panel shows base reflectivity (dBZ), upper right panel shows differential reflectivity (dB), lower left panel shows correlation coefficient (/100), and lower right panel shows differential phase (deg).

a)

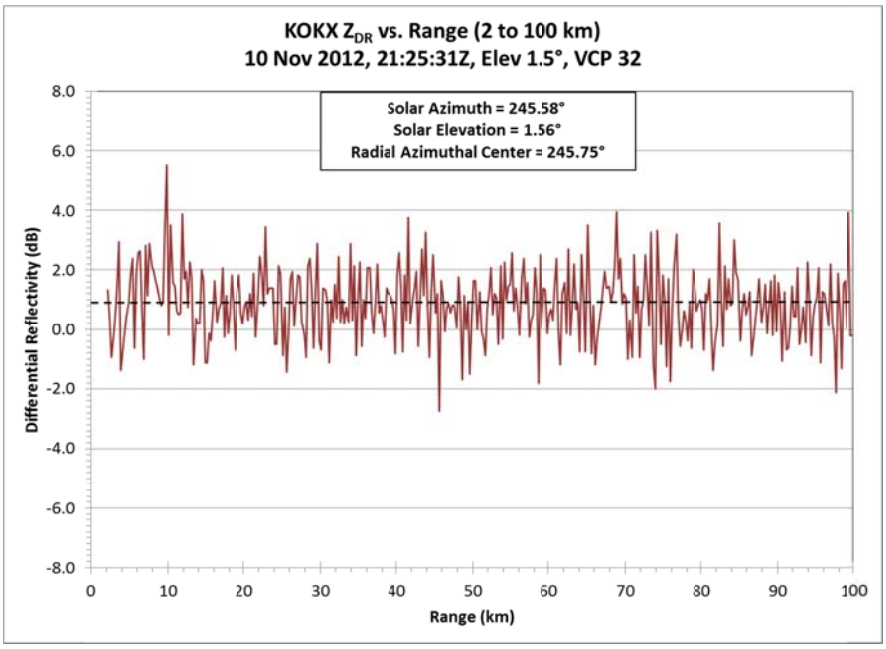

b)

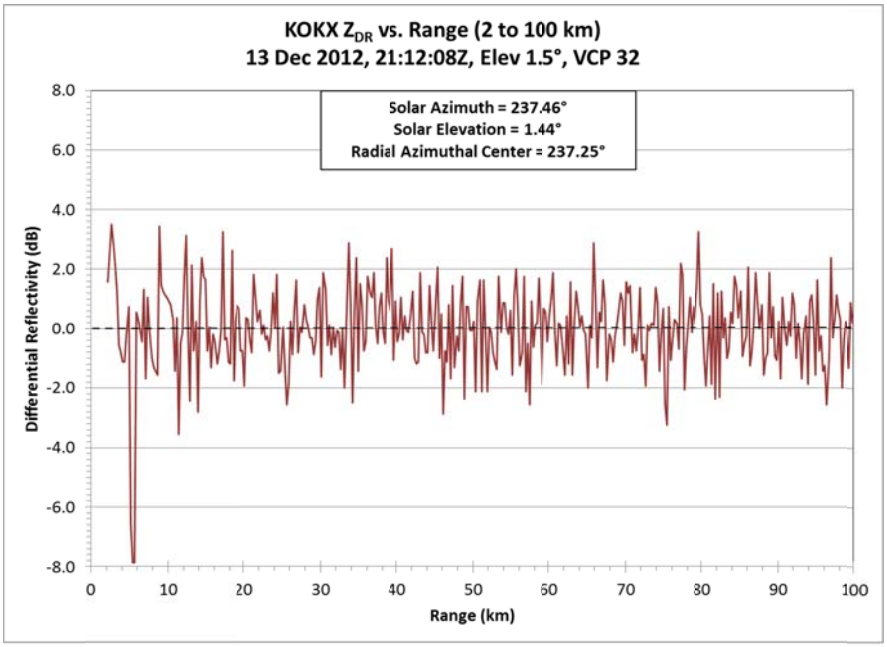

Figures 5a-b. Radial sunspike data. The top image (Fig. 5a) shows a plot of Z_{DR} (dB) values for the Upton, NY WSR-88D (KOKX) from November 10, 2012 around sunset (21:26 UTC). Radial is centered on 245.75° azimuth at 1.5° elevation. The sun's position at the azimuth's time is 1.56° elevation and 245.58° azimuth, a difference of 0.06° in elevation and 0.17° in azimuth. The lower image (Fig. 5b) shows a plot of Z_{DR} values for the same radar around sunset from December 13, 2012 along an azimuth angle centered on 237.25° at 1.5° elevation. The sun's position at the azimuth's time is 1.44° elevation and 237.46° azimuth, a difference of 0.06° in elevation and 0.21° in azimuth. Note the shift of the mean Z_{DR} 0.9 dB downward after major antenna hardware repairs and a full recalibration.

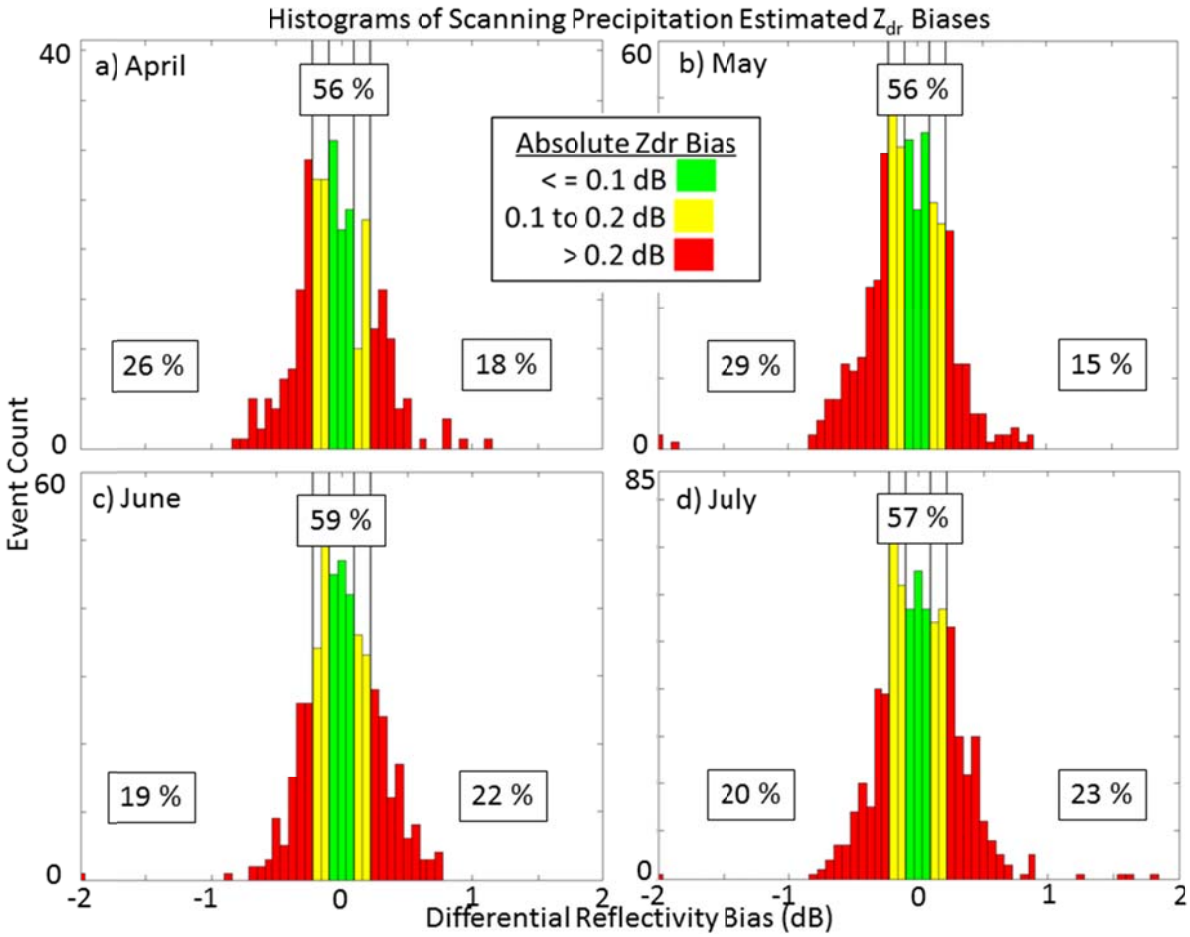

Figure 6. Histograms of scanning "light precipitation" method estimated systematic Z_{DR} biases (fleet wide) for a) April, b) May, c) June, and d) July 2013. Additional histogram data is located in Table 2.

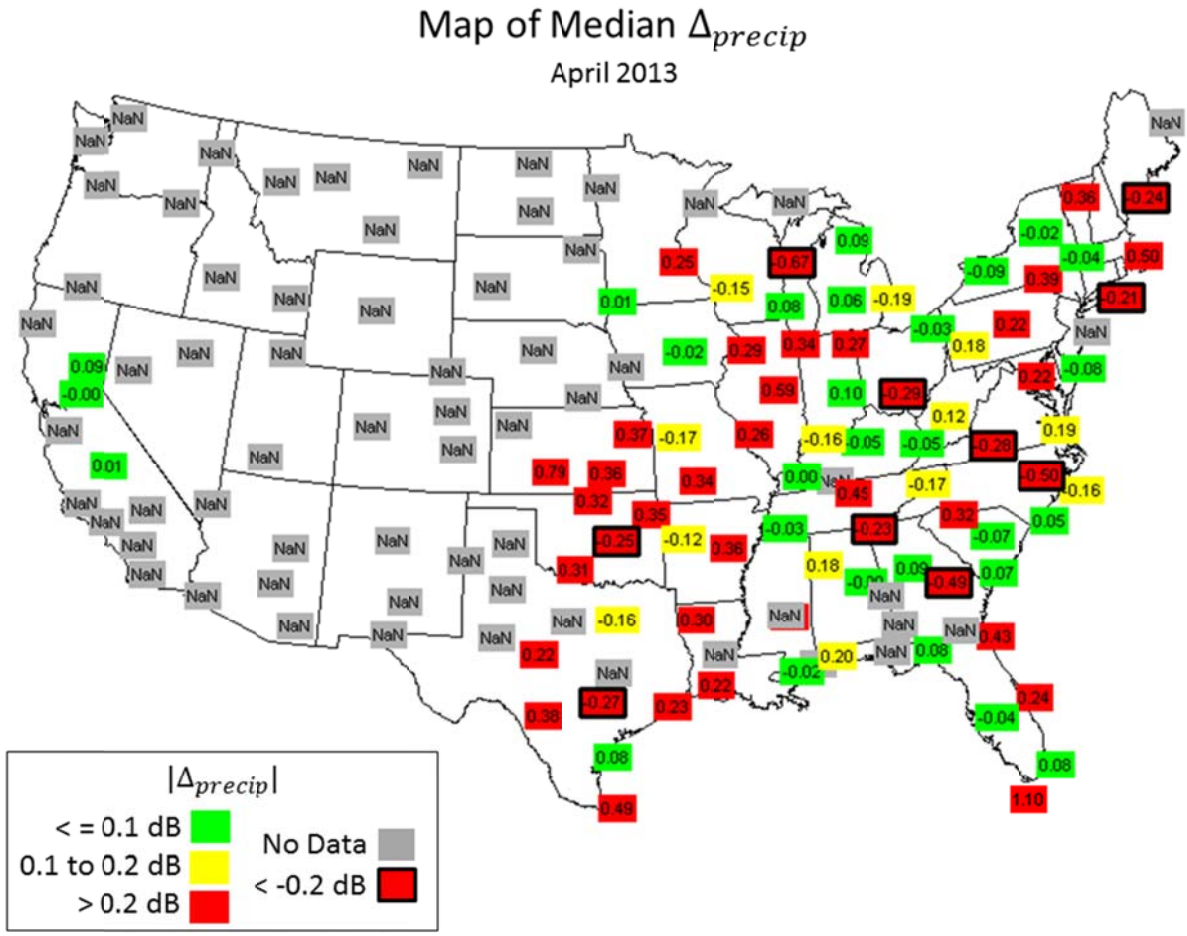

Figure 7. Map of scanning "light precipitation" method estimated systematic Z_{DR} biases at WSR-88D sites for April 2013. Systematic biases are color coded with $|\Delta_{precip}| \leq 0.1\ dB$ as green, $0.1\ dB < |\Delta_{precip}| \leq 0.2\ dB$ as yellow, and $|\Delta_{precip}| > 0.2\ dB$ as red. $\Delta_{precip} < -0.2\ dB$ are color coded red with a black box around the number. Sites labeled "NaN" and colored gray did not have enough data / rain to compute a Δ_{precip} value.

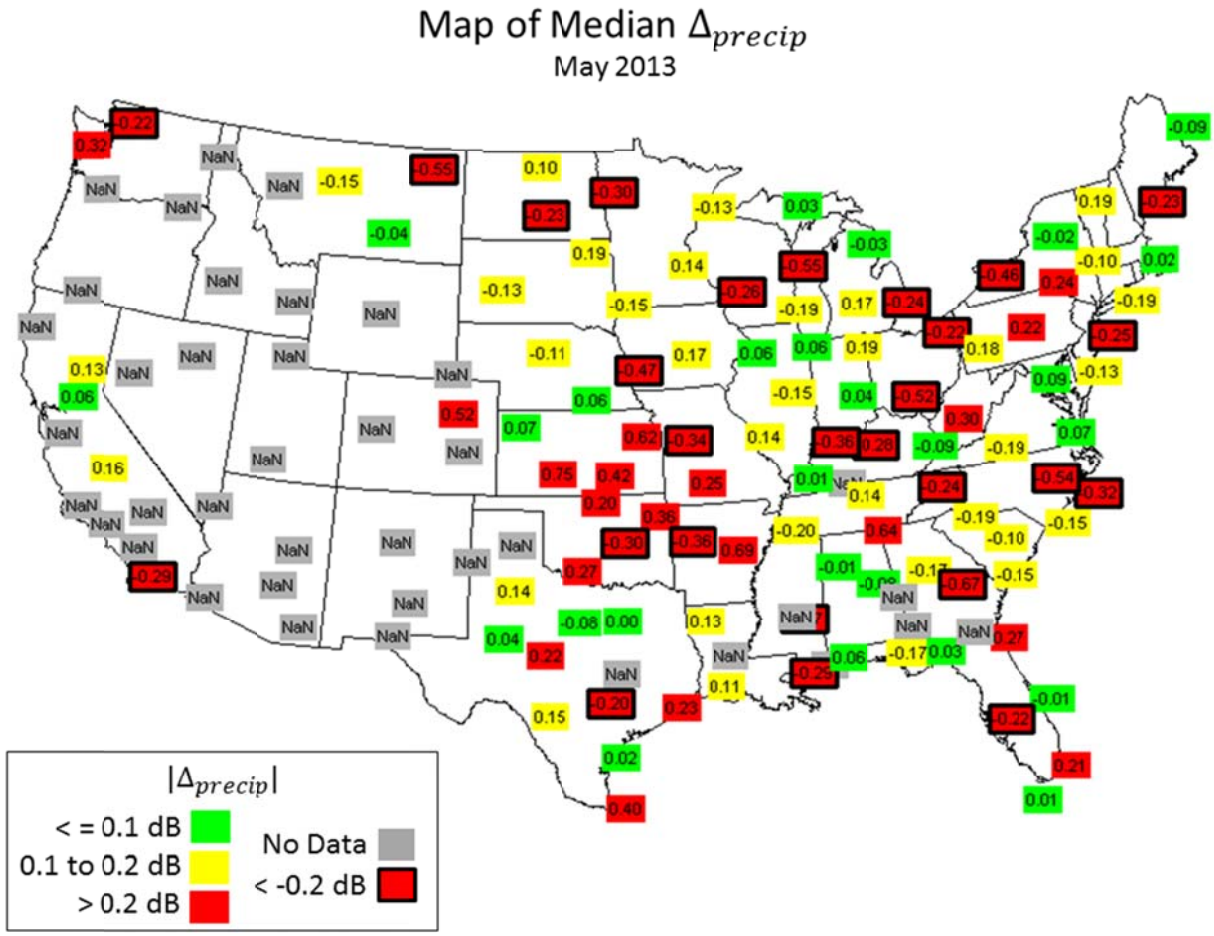

Figure 8. As in Fig. 7, but for May 2013.

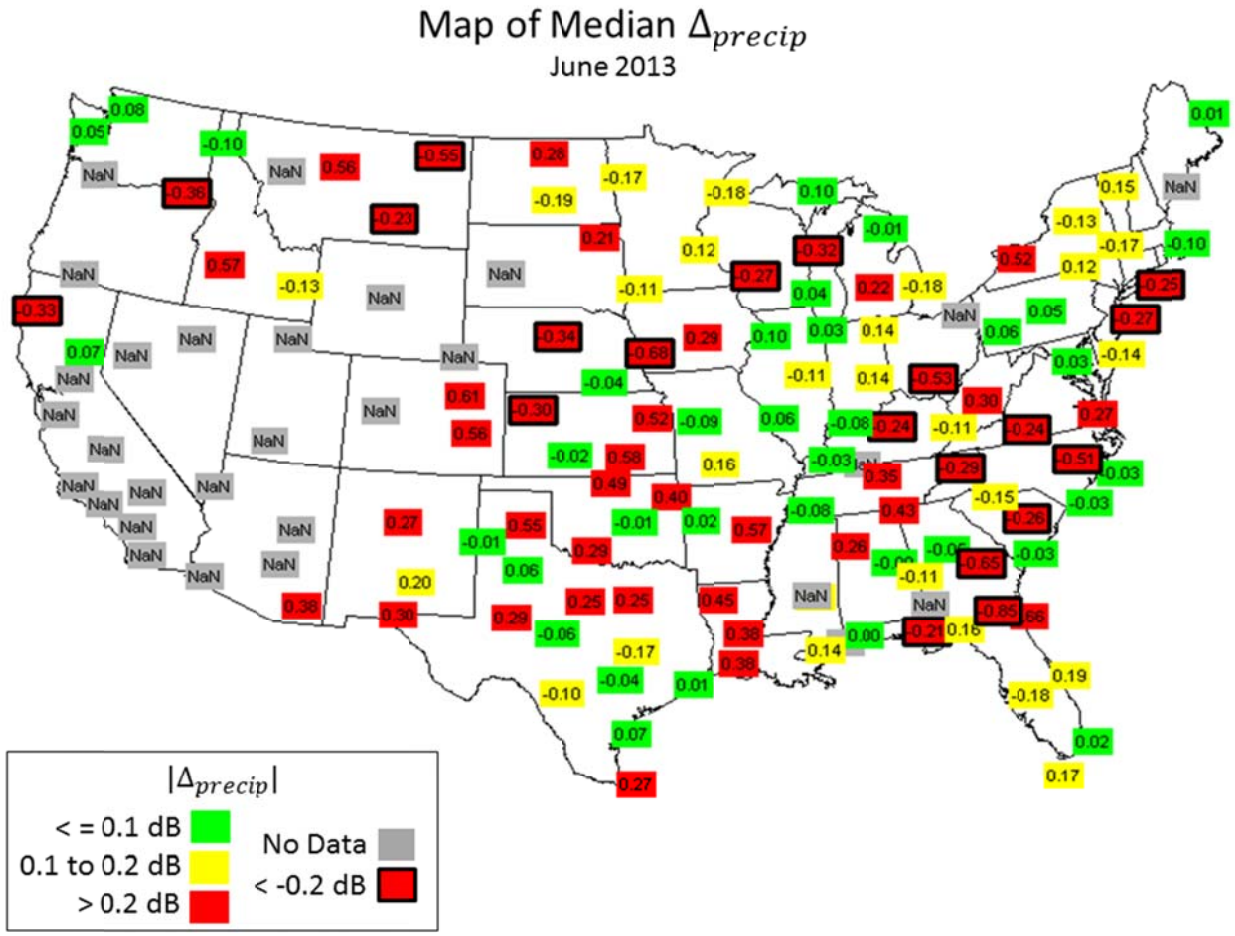

Figure 9. As in Fig. 7, but for June 2013

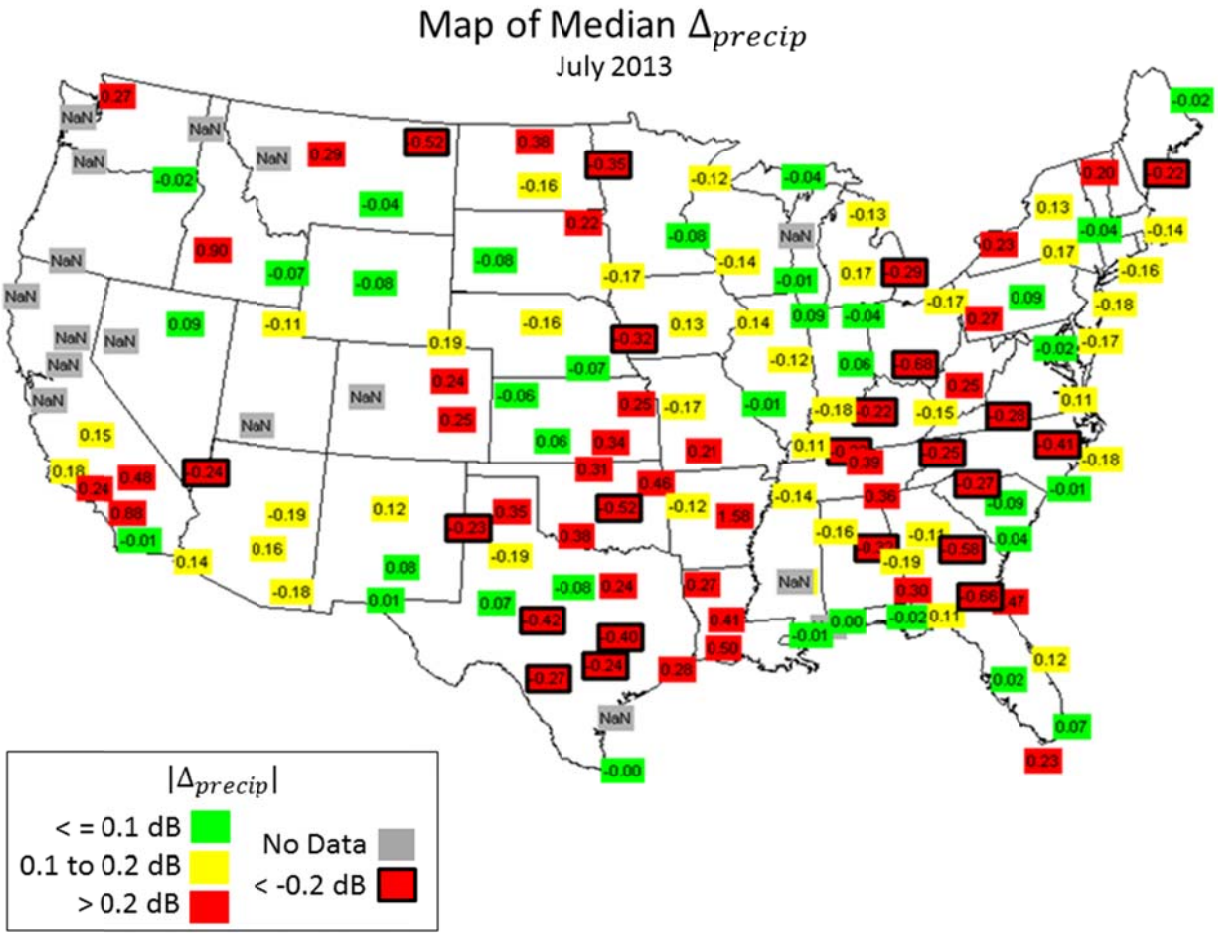

Figure 10. As in Fig. 7, but for July 2013

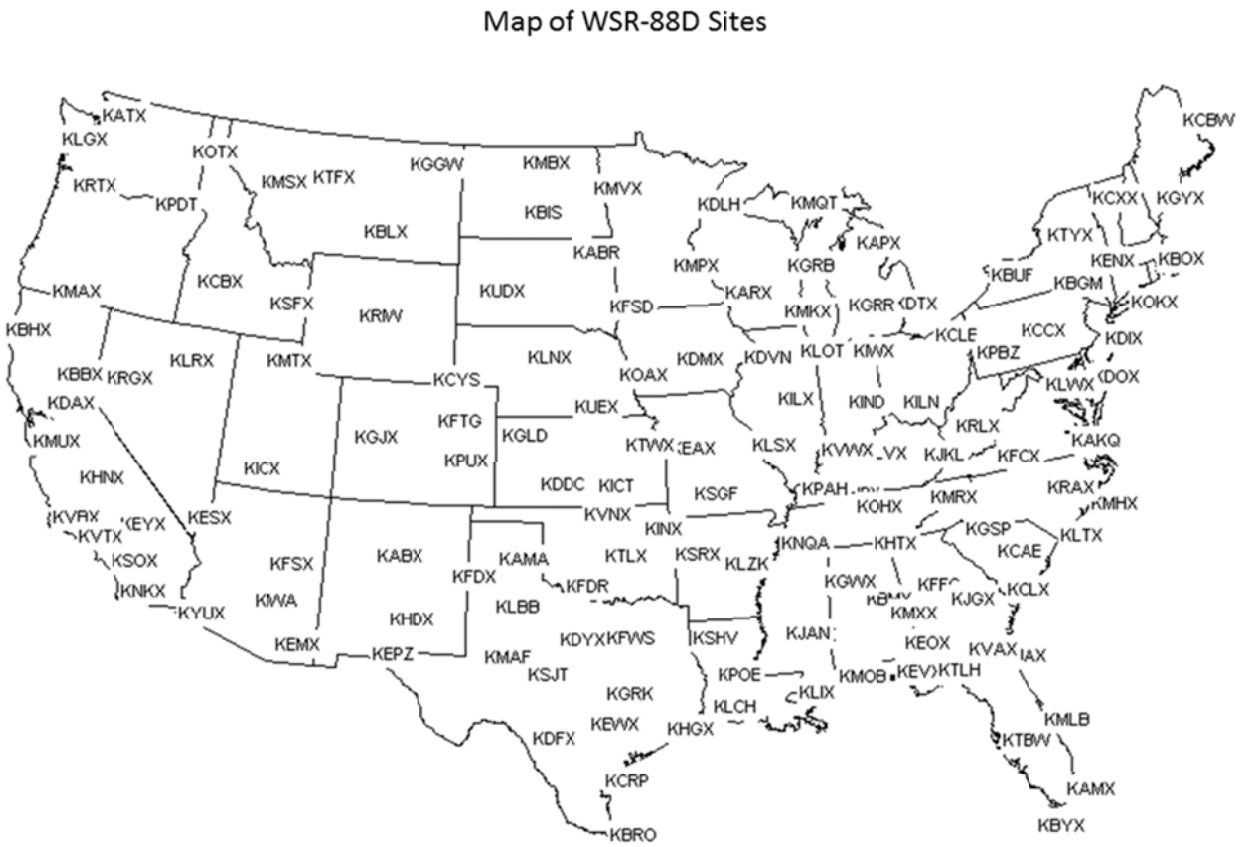

Figure 11. Map of WSR-88D Sites in the contiguous 48 states.

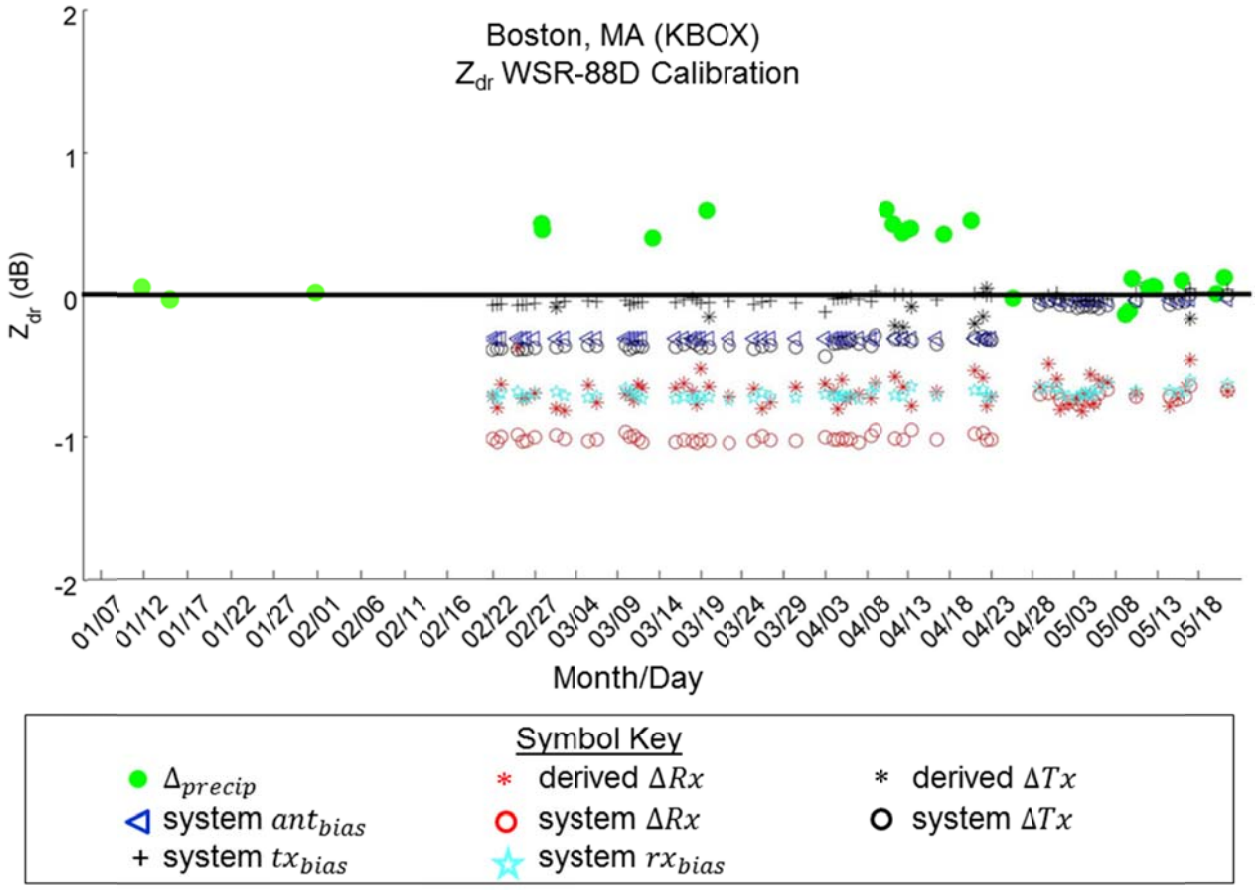

Figure 12. WSR-88D Z_{DR} Calibration time series data for Boston, MA (KBOX). The x-axis is time (month/day) and the y-axis is Z_{DR} (dB). Plotted are Δ_{precip} (green dot), system ant_{bias}, (sideways blue triangle), system tx_{bias}(plus sign), derived ΔRx (red star), system ΔRx (red circle), system rx_{bias}(cyan pentagram), derived ΔTx (black star), and system ΔTx (black circle).

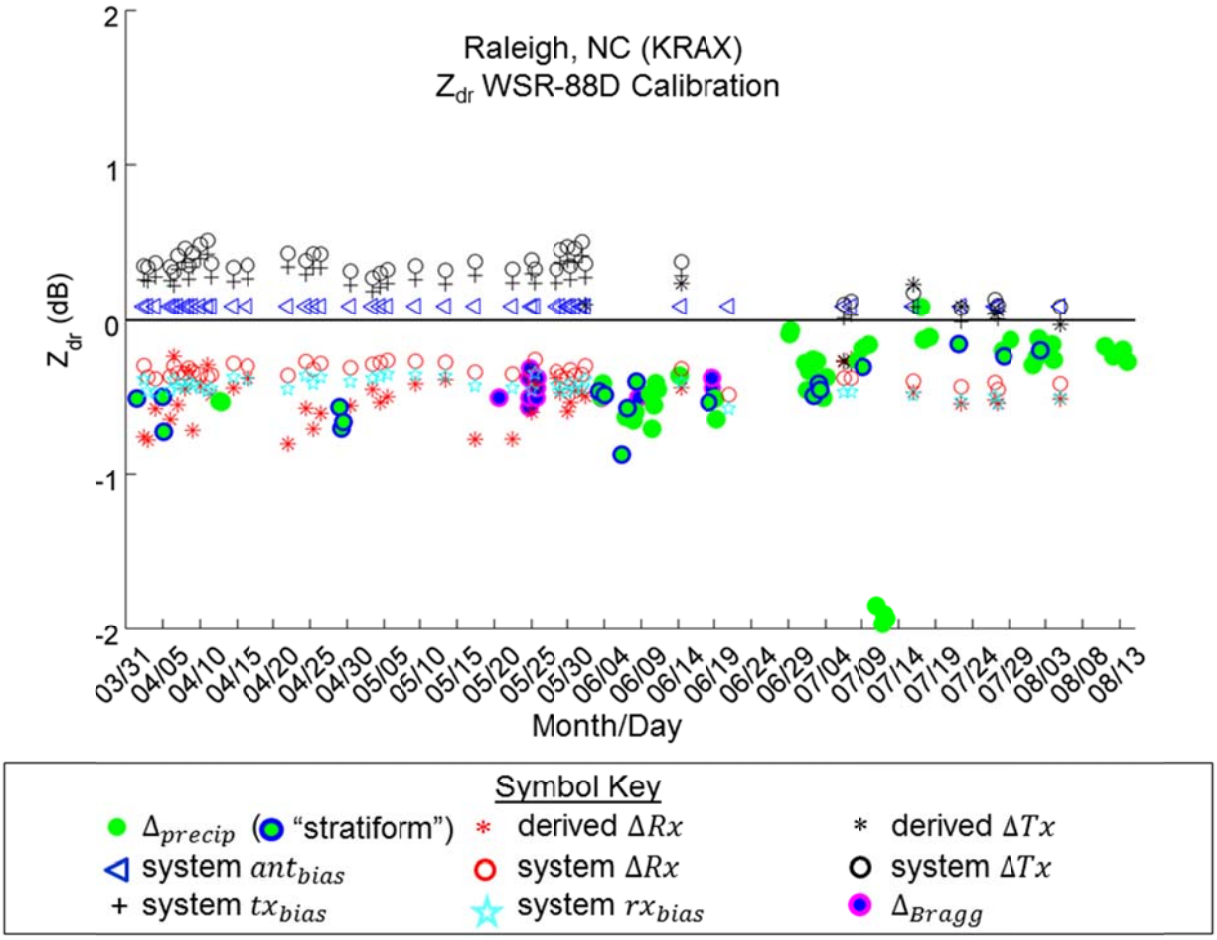

Figure 13. WSR-88D Z_{DR} Calibration time series data for Raleigh, NC (KRAX). The x-axis is time (month/day) and the y-axis is Z_{DR} (dB). Plotted are Δ_{precip} (green dot), system ant_{bias}, (sideways blue triangle), system tx_{bias}(plus sign), derived ΔRx (red star), system ΔRx (red circle), system rx_{bias}(cyan pentagram), derived ΔTx (black star), system ΔTx (black circle), and Δ_{Bragg} (blue dot with magenta circle).

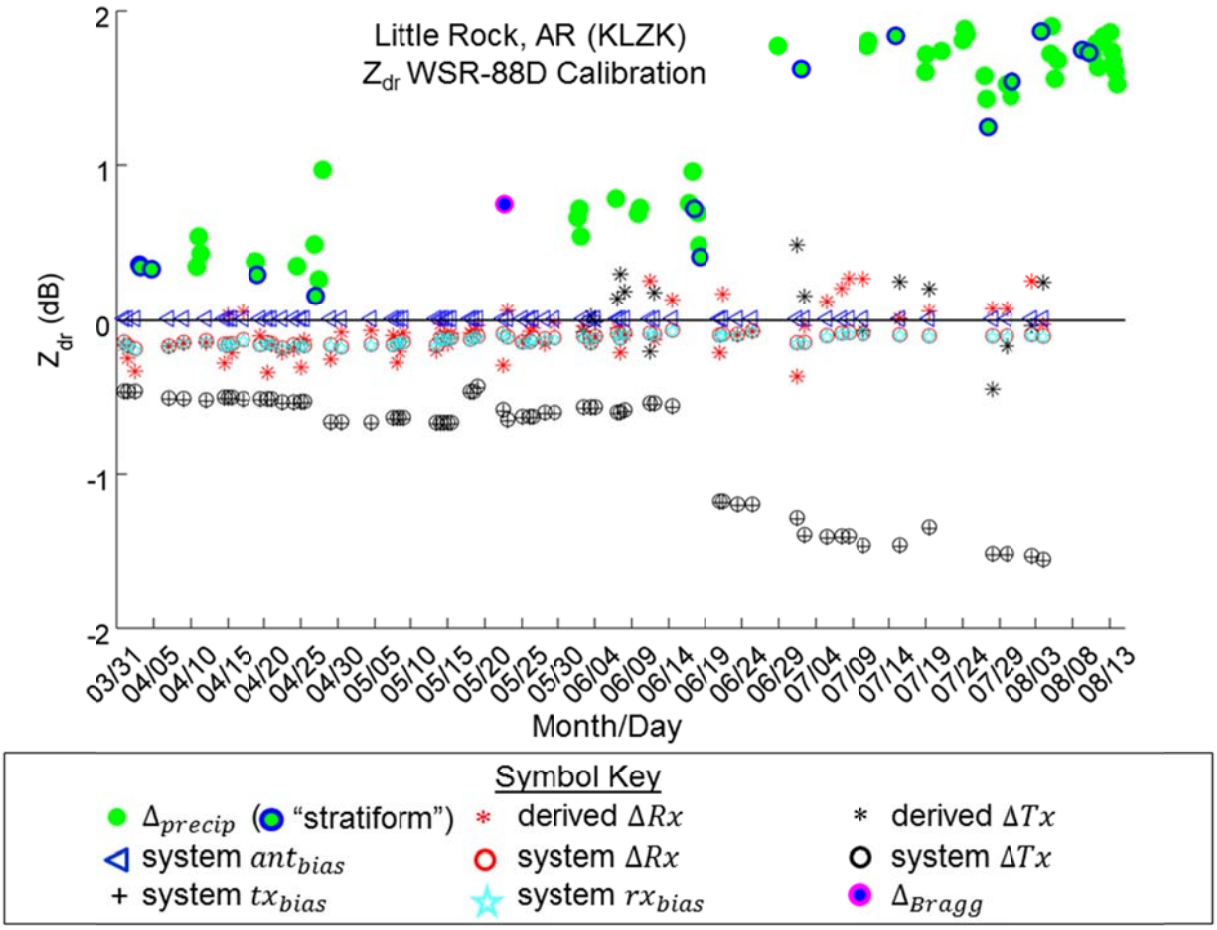

Figure 14. As in Fig. 13, but for Little Rock, AR (KLZK).

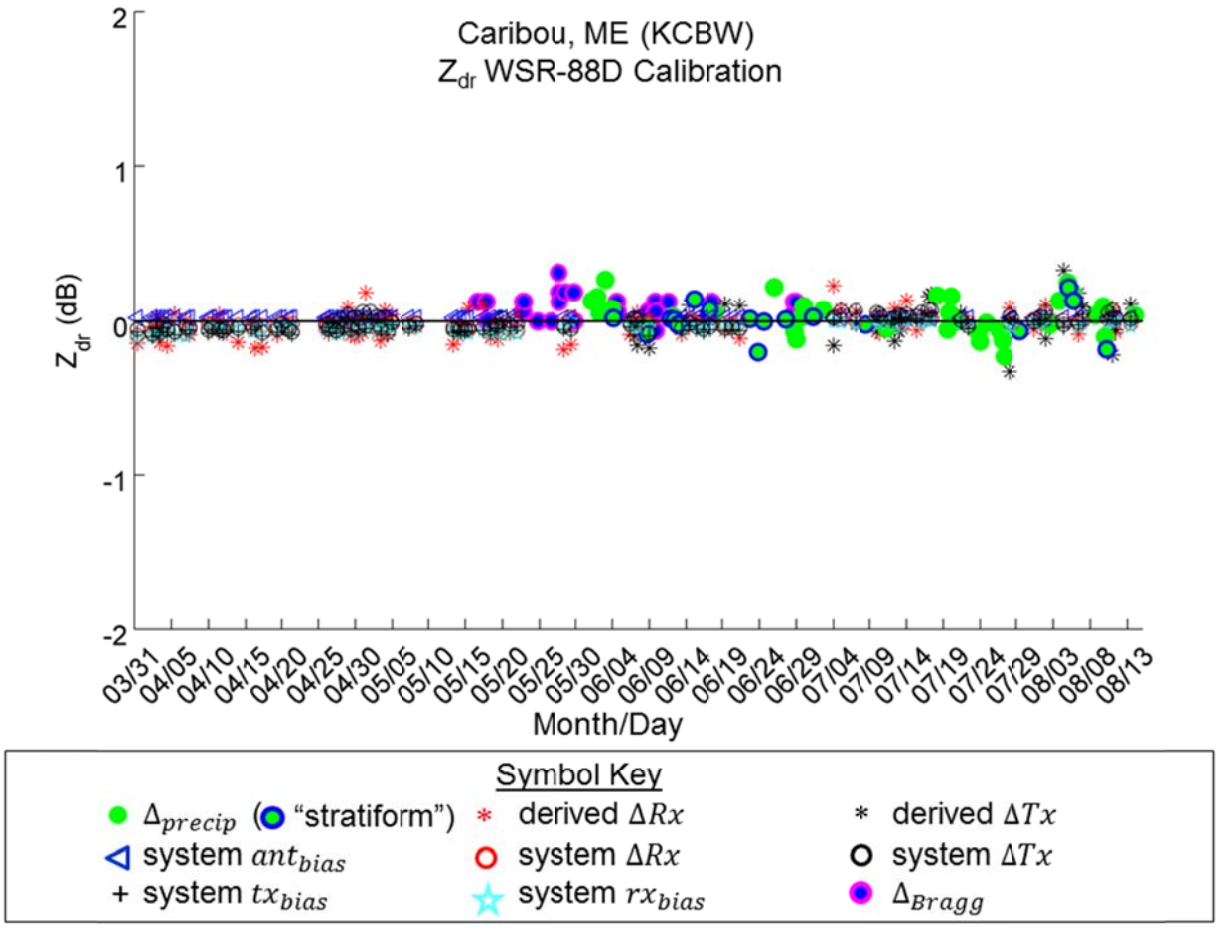

Figure 15. As in Fig. 13, but for Caribou, ME (KCBW).